SEMARAK ILMU PUBLISHING

Journal of Advanced Research in Fluid Mechanics and Thermal Sciences

Journal homepage:
https://semarakilmu.com.my/journals/index.php/fluid_mechanics_thermal_sciences/index
ISSN: 2289-7879

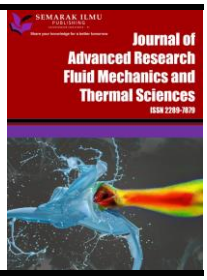

Bi-stability Study of Double Diffusive Convection Using the Carreau-Yasuda Model in a Shallow Horizontal Porous Layer Filled with a Non-Newtonian Fluid

Sara Bensilakhal[1,2], Redha Rebhi[3,4], Noureddine Hadidi[1,2], Giulio Lorenzini[5,*], Yacine Kerchiche[6], Younes Menni[7], Houari Ameur[7], Hijaz Ahmad[8,9]

[1] Laboratoire Matériaux et Environnement, LME, Université de Médéa, 26000 Médéa, Algeria
[2] Department of Process Engineering and Environment, Faculty of Technology, University of Medea, Medea 26000, Algeria
[3] Department of Mechanical Engineering, Faculty of Technology, University of Medea, Medea 26000, Algeria
[4] LERM-Renewable Energy and Materials Laboratory, University of Medea, Medea 26000, Algeria
[5] Department of Engineering and Architecture, University of Parma, Parco Area delle Scienze, 181/A, 43124 Parma, Italy
[6] National Polytechnic School of Algiers, Algeria
[7] Department of Technology, University Center Salhi Ahmed Naama (Ctr. Univ. Naama), P.O. Box 66, Naama 45000, Algeria
[8] Near East University, Operational Research Center in Healthcare, Near East Boulevard, PC: 99138 Nicosia/Mersin 10, Turkey
[9] Section of Mathematics, International Telematic University Uninettuno, Corso Vittorio Emanuele II, 39, 00186 Roma, Italy

ARTICLE INFO

Article history:
Received 20 May 2022
Received in revised form 20 October 2022
Accepted 6 November 2022
Available online 26 November 2022

Keywords:
Non-linear convection; porous layer; non-Newtonian liquid; shear-thinning fluid; Bi-stability; Hopf bifurcation

ABSTRACT

The onset of non-linear convection in a horizontal porous layer saturated by a shear-thinning liquid is studied. The Carreau-Yasuda model is utilized for modeling the behavior of the working medium. Constant fluxes of heat and mass are imposed on the horizontal walls of the cavity, while the vertical sides are assumed adiabatic and impermeable. The parallel flow approximation and the finite difference approach are used to conduct the investigation analytically and numerically, respectively. By considering an infinitesimal perturbation, the linear stability analysis of the diffusive and convective states is conducted based on the finite element method. The theory of linear stability is employed to determine the critical Rayleigh number for the onset of motion from the rest state as well as the onset of Hopf bifurcation, transition from the stationary to oscillatory convection. Overall, the Carreau-Yasuda rheological parameters have a significant impact on the thresholds of convection. The most interesting findings of this study is highlighting the existence of a bi-stability phenomenon, i.e., the existence of two steady-state solutions, which was not observed before in non-Newtonian fluids convection.

1. Introduction

Many natural and technological fields use convection with double diffusive in porous media filled with viscous fluids, such as the food industry, filtration processes, polymer engineering, petroleum drilling, biomedical, cosmetic, molding processes, geothermal exploitation, and so on [1-8]. Some works were realized on the convection in differentially heated and salted enclosures filled with

* *Corresponding author.*
E-mail address: lorenzini.unipr@gmail.com

https://doi.org/10.37934/arfmts.101.1.137159

Newtonian fluids. Goyeau *et al.,* [9] inspected the convection in a rectangular porous enclosure, and they proposed correlations for the thermal and mass exchange in the cooperating case. Gobin and Bennacer [10] inspected the two-dimensional double diffusive convection in a cavity, and they focused on the boundary layer regime. Other authors treated the influence of the buoyancy ratio, which varied from 0 to 2, on the thermal exchange in a cavity [11-14]. Kalla *et al.,* [15] treated the problem of convection with double diffusive in a shallow cavity under thermal and mass fluxes. Bahloul *et al.,* [16,17] examined the convection with double diffusive at mixed boundary conditions. The result provided by Mamou [18] on the convection in a shallow porous layer revealed that the thresholds for the convection over stability and Hopf bifurcation were significantly affected by the acceleration coefficient. Rebhi *et al.,* [19,20] investigated the convection generated in porous cavities containing a binary fluid and discovered that the drag parameters had a significant impact on the stability and onset of subcritical and Hopf bifurcation. In a porous layer, the double diffusive and oscillatory natural convection were studied by Attia *et al.,* [21] while considering the Soret and Dufour effects.

There are only a few works on thermo-solutal convection in porous cavities containing non-Newtonian fluids. Bian *et al.,* [22] inspected the impact of shear-thinning behavior on the convection in an inclined porous rectangular cavity. Pericleous [23] examined how shear-thinning and shear-thickening behaviors affected convection in a chamber with vertical walls that were isothermally heated. For complex fluids, Chen and Chen [24] considered the free convection in porous cavity. Mehta and Rao [25,26] characterized the buoyancy-induced flows of complex fluids over a non-isothermal obstacle inserted in a porous cavity. Other authors treated the case of power-law fluids in cavies at different boundary conditions [27-30]. Benouared *et al.,* [31] explored the convection within a Rayleigh-Bénard cavity heated from the bottom. The effect of rheological factors on convection in a shallow porous layer was examined by Khechiba *et al.,* [32]. Rebhi *et al.,* [33] analysed numerically and analytically the rest state stability of Dupuit-Darcy natural convection of binary fluid saturated vertical porous layer. Their main finding was that Hopf bifurcation and subcritical convection affected significantly by the from drag effect, which acts as a stabilizing effect. Alloui and Vasseur [34] and Krishna and Reddy [35] considered the case of Carreau-Yasuda modeled fluids. Rebhi *et al*., [36] to determine how Rayleigh-Bénard thermosolutal convection instabilities in shallow and finite aspect ratio enclosures were impacted by the rheological behaviour of non-Newtonian fluids. They showed that the bistability convective regime exists for every aspect ratio of the enclosure, irrespective of the type of thermal and solutal boundary conditions. Lounis *et al*., [37] investigated the impact of Dufour and Soret effects on a double-diffusive convection in an inclined square enclosure using the Carreau-Yasuda model for modeling the rheological behavior of the non-Newtonian fluid. Their main finding was that for different power-law index values, the Lewis number increases the heat and mass exchange.

In our knowledge, the impact of the fluid rheological behavior and the buoyancy forces on the thresholds of bifurcations has not been studied previously. Therefore, the purpose of this work is to examine the impact of shear-thinning behavior of complex fluids on the convection with double diffusive in a horizontal porous enclosure. The structure of the essay is as follows. The problem formulation is described in section 2. The numerical approach used to solve the complete nonlinear governing equations is detailed in section 3. In section 4, the crucial Marangoni and Rayleigh numbers for the onset of motion from rest are predicted using the parallel flow theory. The commencement of motion from rest as well as the onset of Hopf oscillatory convection are predicted using a linear stability analysis in section 5. Section 6 discusses the results as a function of the governing parameters after the results are presented in terms of stream function, temperature profiles, and heat transfer. Some final thoughts are contained in the last section.

2. Case Study

The situation under study is a non-Newtonian fluid-saturated horizontal porous layer with dimensions of length L' and height H', Figure 1. While the left and right-side walls are insulated, the horizontal surfaces have constant concentration and temperature values. The physical parameters are taken to be constant while the fluid's viscous dissipation is ignored.

The following equations express the conservation of energy, momentum, and solute balances

$$\nabla^2\psi' = -\frac{gK\beta_T}{\nu}\frac{\partial}{\partial x'}\left(T' + \frac{\beta_S}{\beta_T}S'\right) \tag{1}$$

$$(\rho C)_p \frac{\partial T'}{\partial t'} + (\rho C)_f V'.\nabla T' = k\nabla^2 T' \tag{2}$$

$$\phi\frac{\partial S'}{\partial t'} + V'.\nabla S' = D\nabla^2 S' \tag{3}$$

where V' is the Darcy velocity, g is the gravitational acceleration, ν is the kinematic viscosity, K is the porous matrix permeability, β_T and β_S are the thermal and concentration expansion coefficients, $(\rho C)_p$ and $(\rho C)_f$ are the saturated porous medium's and the fluid's respective heat capacities, k and D are the species thermal conductivity and mass diffusivity, ϕ is the porous medium's porosity and, the stream function ψ' is defined such that $u' = \partial\psi'/\partial y'$ and $v' = -\partial\psi'/\partial x'$.

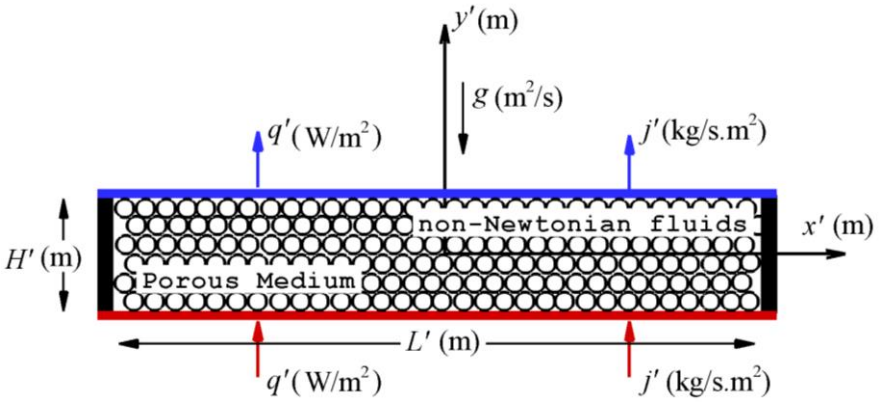

Fig. 1. Situation of the flow and system of coordinates

In order to represent non-Newtonian fluids, the Carreau-Yasuda model is given by [38]

$$\frac{\mu-\mu_\infty}{\mu_0-\mu_\infty} = [1 + (\lambda'\dot{\gamma}')^a]^{(n-1)/a} \tag{4}$$

where μ_0 and μ_∞ represent the viscosities at low and high shear rates, respectively, $n < 1$ represents the shear-thinning index, λ' represents the fluid's time characteristic, $\dot{\gamma}'$ represents the shear rate's magnitude, and a is a dimensionless parameter that describes the transition between the zero-shear-rate region and the power-law region. These non-dimensional variables are utilized

$$(x,y) = \frac{(x',y')}{H'}, t = \frac{t'\alpha}{\sigma H'^2}, (u,v) = \frac{(u',v')H'}{\alpha}\ ,\ \sigma = \frac{(\rho C)_p}{(\rho C)_f},\ \alpha = \frac{Le}{Pr},\ \psi = \frac{\psi'}{\alpha},\ \varepsilon = \frac{\phi}{\sigma},\ T = \frac{(T'-T_0')}{\Delta T^*},\quad S = \frac{(S'-S_0')}{\Delta S^*},\ \ q' = -k\nabla T', j' = -\rho D\nabla S',\ \Delta T^* = \frac{q'H'}{k}, \Delta S^* = \frac{j'H'}{\rho_0 D}, \mu_{CY} = \frac{\mu}{\mu_0},\ \ \lambda_{CY} = \frac{\lambda'\alpha}{\varepsilon H'^2} \tag{5}$$

where ρ_0 is the fluid mixture density at temperature $T' = T'_0$ and species fraction $S' = S'_0$. The subscript 0 refers to condition at the origin of the coordinate system.

The following are the dimensionless governing Eq. (1) to Eq. (3)

$$\frac{\partial}{\partial x}\left(\mu_{CY}\frac{\partial \psi}{\partial x}\right) + \frac{\partial}{\partial y}\left(\mu_{CY}\frac{\partial \psi}{\partial y}\right) = -R_T\frac{\partial}{\partial x}(T + \phi S) \tag{6}$$

$$\frac{\partial T}{\partial t} + \frac{\partial \psi}{\partial y}\frac{\partial T}{\partial x} - \frac{\partial \psi}{\partial x}\frac{\partial T}{\partial y} = \nabla^2 T \tag{7}$$

$$\varepsilon\frac{\partial S}{\partial t} + \frac{\partial \psi}{\partial y}\frac{\partial S}{\partial x} - \frac{\partial \psi}{\partial x}\frac{\partial S}{\partial y} = Le^{-1}\nabla^2 S \tag{8}$$

The behavior of the working medium is defined using the Carreau-Yasuda model, where viscosity, μ_{CY}, is supplied by

$$\mu_{CY}(\dot{\gamma}) = s + (1-s)[1 + (\lambda_{CY}|\dot{\gamma}|)^a]^{(n-1)/a} \tag{9}$$

where μ_{CY} is the dimensionless shear-dependent apparent viscosity, $s = \mu_\infty/\mu_0$ is the ratio of infinite-to zero-shear-rate viscosities.

As written, the dimensionless rate-of-strain $\dot{\gamma}$ is

$$\dot{\gamma} = \left[4\left(\frac{\partial^2 \psi}{\partial x \partial y}\right)^2 + \left(\frac{\partial^2 \psi}{\partial y^2} - \frac{\partial^2 \psi}{\partial x^2}\right)^2\right]^{1/2} \tag{10}$$

The system's walls are subjected to the equivalent dimensionless boundary conditions, which are

$$x = \pm\frac{A}{2}, \quad \psi = 0, \quad \frac{\partial T}{\partial x} = \frac{\partial S}{\partial x} = 0 \tag{11}$$

$$y = \pm\frac{1}{2}, \quad \psi = 0, \quad \frac{\partial T}{\partial y} = \frac{\partial S}{\partial y} = -1 \tag{12}$$

In the above equations one notice the presence of nine dimensionless parameters, namely the Darcy-Rayleigh number, R_T, the buoyancy ratio, φ, the Lewis number, Le, the normalized porosity, ε, and the aspect ratio of the enclosure, A, expressed as

$$R_T = \frac{\rho_0 \beta_T \Delta T' K H'}{\mu_0 \alpha}, \ \varphi = \frac{\beta_S \Delta S^*}{\beta_T \Delta T^*}, \ Le = \frac{\alpha}{D}, \ A = \frac{L'}{H'} \tag{13}$$

and the Carreau-Yassuda parameters, namely, n, λ_{CY}, a and s.

The computation of heat and mass transfer rates in terms of the local and average Nusselt (Nu,Nu_m) and Sherwood numbers (Sh,Sh_m) is of relevance from an engineering perspective. The Nusselt and Sherwood numbers are calculated using the following method in the current notation

$$Nu^{-1} = \Delta T = T_{(0,-1/2)} - T_{(0,1/2)} \quad \text{and} \quad Sh^{-1} = \Delta S = S_{(0,-1/2)} - S_{(0,1/2)} \tag{14}$$

$$Nu_m = A^{-1}\int_{-A/2}^{A/2} Nu dx \quad \text{and} \quad Sh_m = A^{-1}\int_{-A/2}^{A/2} Sh dx \tag{15}$$

3. Numerical Solution

In order to perform numerical simulations, the differential nonlinear equations governing the problem must be converted to algebraic equations. As a result, a second-order central finite difference technique is used to discretize the equations. Line-by-line iteration is used to solve the algebraic equations. For simulations of double diffusive systems, a *FORTRAN* code was created. Eq. (7) and Eq. (8)'s energy and species were resolved using the alternating-direction implicit approach (ADI). The relaxation factor was varied between 0 and 1. Depending on the settings of the governing parameters, the time step values were between 10^{-2} and 10^{-4}. The convergence criterion for the governing equation is $\left|\sum_{i;j}^{m}\psi_{i,j}^{k+1}-\sum_{i;j}^{m}\psi_{i,j}^{k}\right| / \left|\sum_{i;j}^{m}\psi_{i,j}^{k+1}\right| \leq 10^{-8}$, where, $\psi_{i,j}^{k}$, is the stream function value at the node (i, j) at the iteration, k^{th}. The parallel flow approximation is compared with the numerical solution grid sensitivity in Table 1 for $A=10$, $R_T=50$, $Le=5$, $\varphi=-0.1$, $n=0.4$, $\lambda_{CY}=0.1$, $a=2$ and $s=10^{-2}$. The mesh size of 100×200 is selected as optimal.

Table 1
Comparison of the numerical and analytical solutions and grid sensitivity research for $A=10$, $R_T=50$, $Le=5$, $\varphi=-0.1$, $n=0.4$, $\lambda_{CY}=0.1$, $a=2$ and $s=10^{-2}$

Numerical					Parallel flow
$N_x \times N_y$	60×120	80×160	100×200	120×240	approximation
ψ_0	1.379	1.389	1.396	1.399	1.395
Nu	1.714	1.728	1.736	1.739	1.737
Sh	4.824	4.919	4.973	5.005	5.061
μ_{CY}	0.789	0.787	0.786	0.786	0.786

4. Nonlinear Analytical Solution

An approximate analytical solution, based on the parallel flow approximation was given by numerous authors for the convection in a cavity with a large aspect ratio [30,39,40]. Only the primary steps are provided in this document. This method assumes that the convective flow is parallel to the horizontal walls in the cavity's core zone for the current problem. As a result, the horizontal velocity now only depends on y with the vertical velocity being ignored. The estimated stream function, temperature, and concentration are as follows: $\psi(x,y)\approx\psi(y)$, $T(x,y)\approx C_T x+\theta_T(y)$ and $S(x,y)\approx C_S x+\theta_S(y)$, where C_T and C_S are, respectively, unknown constant temperature and concentration gradients in the $\mathrm{x}-$direction, θ_T and θ_s are the temperature and concentration profiles. Utilizing these approximations in Eq. (6) to Eq. (8), we get

$$\frac{d}{dy}\left(\mu_{CY}\frac{d\psi}{dy}\right)=-R_T(C_T+\varphi C_S) \tag{16}$$

$$\frac{d^2T}{dy^2}=C_T\frac{d\psi}{dy} \tag{17}$$

$$\frac{d^2S}{dy^2}=Le^{-1}C_S\frac{d\psi}{dy} \tag{18}$$

and the apparent viscosity (μ_{CY}), Eq. (9) is now given by

$$\mu_{CY}(\dot{\gamma})=s+(1-s)[1+(\lambda_{CY}|\dot{\gamma}|)^a]^{(n-1)/a} \tag{19}$$

where the shear rate ($\dot{\gamma}$), Eq. (10), is reduced to

$$\dot{\gamma} = \left|\frac{\partial^2 \psi}{\partial y^2}\right| \tag{20}$$

Any transversal section's heat and species transport rates are provided by

$$C_T = 2\int_0^{1/2} u(y)\theta_T(y)\,dy \quad \text{and} \quad C_S = 2Le\int_0^{1/2} u(y)\theta_S(y)\,dy \tag{21}$$

The impact of the porous layer aspect ratio on the apparent viscosity, μ_{CY}, profile at $x = 0$ for $Le = 5$, $\varphi = -0.1$, $n = 0.8$, $\lambda_{CY} = 0.2$, $a = 2$ and $s = 10^{-2}$ is demonstrated in Figure 2. From the figure, with increasing the aspect ratio from 1 to 10, it appears clearly that the apparent viscosity toward a constant value along the vertical walls ($y = \pm 0.5$).

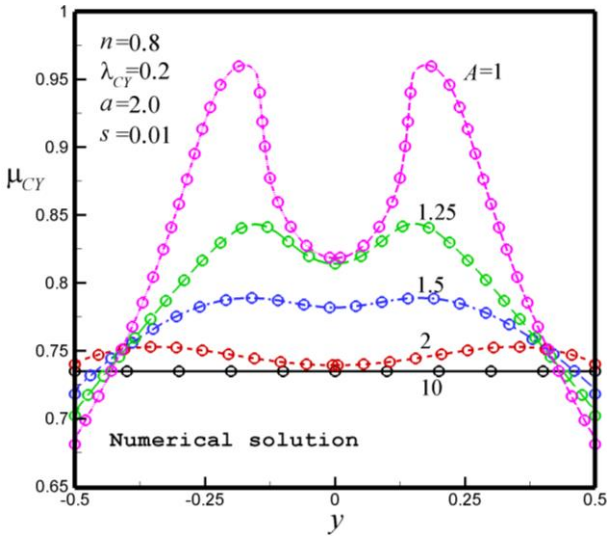

Fig. 2. Aspect ratio effect on the predicted apparent viscosity, μ_{CY}, profile obtained for $R_T = 50$, $Le = 5$, $\varphi = -0.1$ and $\varepsilon = 1$

In this situation, Eq. (16) to Eq. (18) may be solved analytically when the viscosity apparent (μ_{CY}) is assumed constant. Hence, the momentum equation, Eq. (16), was reduced

$$\frac{d^2\psi}{dy^2} = -\Re \tag{22}$$

where: $\Re = R_T(C_T + \varphi C_S)/\mu_{CY}$. The solution of Eq. (22) is obtained as follow

$$\psi(y) = \Re\left(\frac{1}{8} - \frac{y^2}{2}\right) \tag{23}$$

From Eq. (23), the velocity field, $u = \partial\psi/\partial y$, derived from the stream function is given by the following expression

$$u(y) = -\Re y \tag{24}$$

From Eq. (19), the apparent viscosity, μ_{CY}, can be written as follows

$$\mu_{CY} = s + (1-s)[1 + (\lambda_{CY}|\Re|)^a]^{n-1/a} \tag{25}$$

The temperature and concentration profiles are obtained by the following solutions

$$T(x,y) = C_T x - C_T \Re\left(\frac{y}{8} - \frac{y^3}{6}\right) - y \tag{26}$$

$$S(x,y) = C_S x - LeC_S \Re\left(\frac{y}{8} - \frac{y^3}{6}\right) - y \tag{27}$$

The constant gradients of C_T and C_S, corresponding to the gradients of temperature and concentration along the x-direction, are stated as

$$C_T = \frac{10\Re}{120+\Re^2} \quad \text{and} \quad C_S = \frac{10Le\Re}{120+Le^2\Re^2} \tag{28}$$

The expressions for the Nu and Sh numbers are shortened to

$$Nu = \frac{12\Re^2+1440}{2\Re^2+1440} \quad \text{and} \quad Sh = \frac{12\Re^2Le^2+1440}{2\Re^2Le^2+1440} \tag{29}$$

Substituting the above expressions of C_T and C_S, Eq. (28), in the expression of $\Re = R_T(C_T + \varphi C_S)/\mu_{CY}$, we obtain the following expression

$$\frac{10R_T\Re}{\mu_{CY}}\left[\frac{1}{120+\Re^2} + \varphi\frac{Le}{120+Le^2\Re^2}\right] - \Re = 0 \tag{30}$$

The threshold for the onset of motion, expressed in terms of the supercritical Rayleigh number, R_{TC}^{sup}, is obtained with the limit $\Re \to 0$, and the subcritical Rayleigh number, R_{TC}^{sub}, and the two turning points (R_{TC}^{tur1} and R_{TC}^{tur2}) are obtained by deriving Eq. (30) with respect to R_T with the limit condition $d\Re/dR_T = \infty$ at the saddle-node point. The critical Rayleigh numbers are expressed as follows

$$R_{TC}^{sup} = \frac{\mu_{CY}R^{sup}}{1+\varphi Le} \tag{31}$$

$$R_{TC}^{sub}\left(R_{TC}^{tur1,2}\right) = \frac{\mu_{CY}^2\mathcal{A}^2\ell^2}{10\lambda} \tag{32}$$

where

$$\begin{aligned}\lambda &= -\lambda_{CY}(n-1)(1-s)(\lambda_{CY}[1+(\lambda_{CY}|\Re|)^a]^{\chi}(\ell\mathcal{A}+\varphi Le\mathcal{A}^2)\ell\Re + \\ &\mu_{CY}[\ell^2(120-\Re^2)+\varphi\mathcal{A}^2Le(120-\Re^2Le^2)] \\ \mathcal{A} &= 120+\mu_{CY}^2, \quad \ell = 120+Le^2\mu_{CY}^2, \quad \chi = \frac{n-1}{a}-1\end{aligned} \tag{33}$$

For an infinite horizontal layer, the constant R^{sup}, in Eq. (31), is computed accurately and is given by $R^{sup} = 12$. This result is independent of the type of thermal and solutal boundary conditions applied to the system's horizontal walls.

5. Linear Stability Analysis: Formulation and Procedure

The linear stability study yielded the critical Rayleigh numbers for the initiation of convection of a non-Newtonian fluid, which are influenced by the wave vector's shape. This section studies the stability of both the convective and the motionless phases. The overall convective solution consists of a basic solution $(\psi, T, S)_b$, that represents the pure diffusive state solution or the steady-state convective solution, and a perturbation solution $(\psi, T, S)_p$. The basic flow solution could be the rest state solution $\psi_b = 0$ and $T_b = -y$ and $S_b = -y$ or the steady-state convective solution derived in the previous section, $\psi_b(x,y) \approx \psi(y)$, $T_b(x,y) \approx C_T x + \theta_T(y)$ and $S_b(x,y) \approx C_S x + \theta_S(y)$.

The global flow unsteady solution can be assumed to be superposition of a steady state basic flow solution, $\psi_b(x,y)$, $T_b(x,y)$, $S_b(x,y)$, and an unsteady infinitesimal perturbation $\psi_p(x,y,t)$, $T_p(x,y,t)$ and $S_p(x,y,t)$, as illustrated by

$$\begin{aligned} \psi(x,y,t) &= \psi_b(x,y) + \psi_p(x,y,t) \\ T(x,y,t) &= T_b(x,y) + T_p(x,y,t) \\ S(x,y,t) &= S_b(x,y) + S_p(x,y,t) \end{aligned} \tag{34}$$

This assumption enabled the following definition of the perturbations for an infinite porous layer

$$\begin{aligned} \psi_p(x,y,t) &= \psi_0 e^{pt+i\ell x} F(y) \\ T_p(x,y,t) &= \theta_0 e^{pt+i\ell x} G(y) \\ S_p(x,y,t) &= \phi_0 e^{pt+i\ell x} H(y) \end{aligned} \tag{35}$$

where $\ell = n\pi/A$ is the wave number and ℓ is the number of cells, $F(y)$, $G(y)$ and $H(y)$ are functions describing the perturbation profiles, and $p = p_r + ip_i$, is a complex number indicating the growth rate of the perturbation, p_r, and the critical frequency, p_i, and ψ_0, θ_0 and ϕ_0 are unknown infinitesimal amplitudes.

The linearized stability equations are created by substituting (33) into (6) to (8) and ignoring the second-order nonlinear terms.

$$\mu_{CY}(D^2 f - \ell^2 f) - D(\partial\mu_{CY}/\partial\dot{\gamma})_b D\psi_b (D^2 f + \ell^2 f) = i\ell R_T (g + \varphi h) \tag{36}$$

$$pg + i\ell D\psi_b g - i\ell T_b f + C_T Df = D^2 g - \ell^2 g \tag{37}$$

$$\varepsilon ph + i\ell D\psi_b h - i\ell S_b f + C_S Df = Le^{-1}(D^2 h - \ell^2 h) \tag{38}$$

where $D = d/dy$, $f = \psi_0 F$, $g = \theta_0 G$ and $h = \phi_0 H$.

The discretized stability equations are constructed into the global eigenvalue system and then into the global matrix system as follows

$$\begin{bmatrix} [A_\psi] & -R_T[B_\psi] & -R_T\varphi[B_\psi] \\ [B_\theta] & [A_\theta] & 0 \\ [B_\phi] & 0 & Le^{-1}[A_\phi] \end{bmatrix} \begin{Bmatrix} f \\ g \\ h \end{Bmatrix} = -p \begin{bmatrix} 0 & 0 & 0 \\ 0 & [\mathcal{C}_\theta] & 0 \\ 0 & 0 & [\mathcal{C}_\phi] \end{bmatrix} \tag{39}$$

The following steps are taken to obtain the appropriate elementary matrices

$$
\begin{aligned}
&[A_\psi]^e = \int_{-1}^{1} \mu_{CY}\left(\frac{dl_j}{d\zeta}\frac{dl_i}{d\zeta}\frac{2}{\Delta y} + \ell^2 l_j l_i \frac{\Delta y}{2}\right) d\zeta + \\
&\int_{-1}^{1} \left(\frac{\partial \mu_{CY}}{\partial \dot{\gamma}}\right)_b \left(\frac{d^2 l_j}{d\zeta^2}\frac{dl_i}{d\zeta}\frac{8}{\Delta y^3} + \ell^2 l_j \frac{dl_i}{d\zeta}\frac{2}{\Delta y}\right)\frac{\partial \psi_b}{\partial \zeta} d\zeta \\
&[A_\theta]^e = \int_{-1}^{1} \left(\frac{dl_j}{d\zeta}\frac{dl_i}{d\zeta}\frac{2}{\Delta y} + \ell^2 \frac{\Delta y}{2} l_j l_i + i\ell \frac{\partial \psi_b}{\partial \zeta} l_j l_i\right) d\zeta \\
&[A_\phi]^e = \int_{-1}^{1} \left(\frac{dl_j}{d\zeta}\frac{dl_i}{d\zeta}\frac{2}{\Delta y} + \ell^2 \frac{\Delta y}{2} l_j l_i + i\ell Le \frac{\partial \psi_b}{\partial \zeta} l_j l_i\right) d\zeta \\
&[B_\psi]^e = \int_{-1}^{1} i\ell \frac{\Delta y}{2} l_j l_i d\zeta, \quad [B_\theta]^e = \int_{-1}^{1} \left(C_T \frac{dl_j}{d\zeta} - i\ell \frac{\partial T_b}{\partial \zeta} l_j\right) l_i d\zeta \\
&[B_\theta]^e = \int_{-1}^{1} \left(C_T \frac{dl_j}{d\zeta} - i\ell \frac{\partial T_b}{\partial \zeta} l_j\right) l_i d\zeta, \quad [B_\phi]^e = \int_{-1}^{1} \left(C_S \frac{dl_j}{d\zeta} - i\ell \frac{\partial S_b}{\partial \zeta} l_j\right) l_i d\zeta \\
&[\mathcal{C}_\theta]^e = [\mathcal{C}_\phi]^e = \int_{-1}^{1} l_j l_i \frac{\Delta y}{2} d\zeta
\end{aligned}
\tag{40}
$$

5.1 Marginal Stability

In general, the threshold of stationary convection is obtained when marginal stability occurs ($p = 0$). After introducing the boundary conditions in the general linear system, Eq. (39), the eigenvalue problem can be reduced to:

$$[E - \lambda I]\{F\} = 0 \quad \text{with:} \quad E = [A]^{-1}[B_\psi][K]^{-1}[B] \tag{41}$$

where $[I]$ is the identity matrix and $\{F\}$ is the eigenvector.

The above equation has a nontrivial solution $\{F\} \neq 0$, only when the determinant $[E - \lambda I] = 0$, which yields m eigenvalues λ_i reorganized as $\lambda_1 \leq \lambda_2 \leq \ldots \leq \lambda_m$, where λ_m is the maximum eigenvalue and λ_1 is the lowest eigenvalue. Thus, according to Eq. (39), the marginal state corresponding to $p = 0$, from which the critical Rayleigh number for the onset of stationary convection (R_{TC}^{sup}) is obtained as

$$R_{TC}^{sup} = \frac{\mu_{CY} R^{sup}}{(1+\varphi Le)} \tag{42}$$

5.2 Transient Stability

The marginal state of overstability corresponds to the condition, $p_r = 0$. The following is the critical Rayleigh number R_{TC}^{over} that defines the commencement of oscillatory convection

$$R_{TC}^{over} = \frac{\mu_{CY}(\varepsilon Le+1) R^{sup}}{Le(\varepsilon+\varphi)} \tag{43}$$

Only when the equation of R_{TC}^{osc} is determined as follows is it possible for the oscillatory convection mode to exist

$$R_{TC}^{osc} = \frac{\mu_{CY}(\varepsilon Le-1)R^{sup}}{Le(\sqrt{\varepsilon}-\sqrt{-\varphi})^2} \tag{44}$$

5.3 The Convective State's Stability

Study is also done on the transitional threshold. Understandably, the transition to oscillatory flows occurs frequently when the Rayleigh number is very high or when the flow strength increases significantly; the critical value is known as the thresholds of Hopf bifurcation (R_{TC}^{Hopf}). In order to find this bifurcation point, known as a Hopf bifurcation.

Table 2 and Figure 3(a) to Figure 3(c) present the data of the linear stability analysis of the convective state for an infinite horizontal porous layer. These figures show the effects of the power-law index (n) and the time constant, λ_{CY}, on the Hopf bifurcation threshold (R_{TC}^{Hopf}), the wavelength (A_C), and the oscillatory frequency ($f_r = |p_i|/2\pi$), respectively, for $Le = 5$, $\varphi = -0.1$, $a = 2$, $s = 10^{-2}$ and $\varepsilon = 1$.

Table 2
Effects of n, and λ_{CY}, on R_{TC}^{Hopf}, A_C and f, in an infinite horizontal layer for $Le = 5$, $\varphi = -0.1$, $a = 2$, $s = 10^{-2}$ and $\varepsilon = 1$

$\lambda_{CY} = 0.6, a = 2, s = 10^{-2}$				$n = 0.4, a = 2, s = 10^{-2}$			
n	R_{TC}^{Hopf}	A_C	f_r	λ_{CY}	R_{TC}^{Hopf}	A_C	f_r
1.0	662.165	1.282	25.378	1.0	88.372	0.909	46.672
0.8	407.890	1.246	29.226	0.8	99.875	0.895	47.640
0.6	226.070	1.082	37.117	0.6	116.893	0.880	48. 671
0.4	116.893	0.880	48.671	0.4	146.554	0.861	49.924
0.2	59.928	0.770	56.836	0.2	216.765	0.840	51.349
0.0	33.237	0.802	51.191	0.0	662.165	1.282	25.378

It is evident that as the power-law index, n, (the time characteristic of the fluid λ_{CY}) decreases below $n = 1$ ($\lambda_{CY} = 1$), the oscillation frequency (f_r), which served as a destabilizing (stabilizing) flow parameter, increases and the critical Rayleigh number (R_{TC}^{Hopf}), at which a Hopf bifurcation occurs, decreases (increases) significantly. As already mentioned, the situation where $n = 1$ or $\lambda_{CY} = 0$, i.e., the apparent viscosity, μ_{CY}, corresponds to a Newtonian fluid for which $R_{TC}^{Hopf} = 662.165$, $A_C = 1.282$ and $f_r = 25.378$. At the start of the Hopf bifurcation, the stability analysis also produces two conjugate solutions. These two options, which are mirror reflections of one another, might result in waves that travel horizontally.

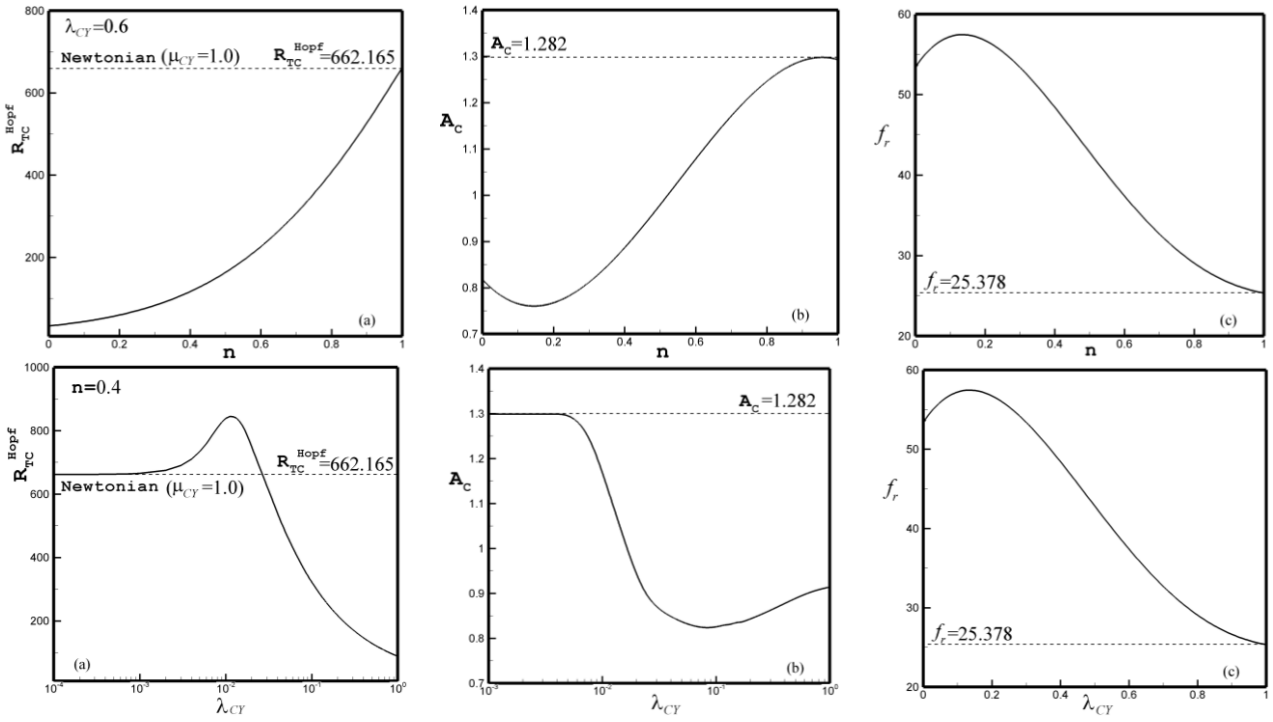

Fig. 3. Effects of n, and λ_{CY}), on: (a) R_{TC}^{Hopf}, (b) A_C and (c) f_r, for $Le = 5$, $\varphi = -0.1$, $a = 2$, $s = 10^{-2}$ and $\varepsilon = 1$

Figure 4 shows the perturbation profiles $n = \lambda_{CY} = 0.6$, $Le = 5$, $a = 2$, $s = 10^{-2}$ and $\varepsilon = 1$ at the beginning of the Hopf bifurcation. The critical values for the set of governing parameters that are being studied here are $R_{TC}^{Hopf} = 226.07$, $A_C = 0.923$ and $p_i = \pm 233.592$ ($f_r = 37.11$).

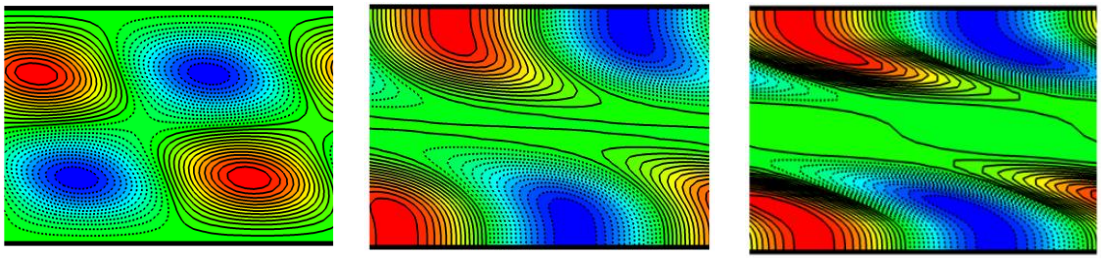

(a) (b) (c)

Fig. 4. Perturbation profiles ψ_p, T_p and S_p at the threshold of Hopf bifurcation, R_{TC}^{Hopf}, for $Le = 5$, $\varphi = -0.1$, $n = \lambda_{CY} = 0.6$, $a = 2$, $s = 10^{-2}$ and $\varepsilon = 1$: $R_{TC}^{Hopf} = 226.07$, $A_C = 0.923$ and $p_i = \pm 233.592$ ($f_r = 37.11$)

6. Findings and Analysis

The purpose of this study is to inspect the impact of the rheological parameters on the convective flow, thermal and mass exchange rates, and on the threshold of supercritical and overstable convection, up to Hopf bifurcation. The following ranges are considered: $10^0 \leq R_T \leq 10^2$, $10^{-2} \leq Le \leq 10^3$, $-0.8 \leq \varphi \leq 0.6$, $0 \leq \varepsilon \leq 1$, $0.1 \leq n \leq 1$, $0 \leq \lambda_{CY} \leq 10$, $1 \leq a \leq 10$ and $0 \leq s \leq 10$.

The numerical and analytical values of ψ, u, T and S are compared at $x = 0$, Figure 5. The results were obtained for $R_T = 50$, $Le = 5$, $\varphi = -0.1$, $\lambda_{CY} = 0.2$, $a = 2$, $s = 10^{-2}$, $\varepsilon = 1$ and various n. A deep insight in these plots reveal a good agreement between both solutions. The flow intensity (ψ)

is clearly decreasing with the rise of, n, and therefore reduce the flow circulation intensity inside the layer, as the fluid becomes more and more shear-thinning ($n < 1$), Figure 5(a). The vertical profiles of u-velocity are symmetric, as observed in Figure 5(b). The velocity is maximum on the wall ($y = \pm 0.5$), it decreases sharply toward $u = 0$ at the enclosure center ($y = 0$) and then it drops back to $u = -u_{max}$ at the wall ($y = 0.5$). The impact of *n* on the temperature and concentration profiles is depicted in Figure 5(c) and Figure 5(d). The temperature and concentration near the solid sides are intensified with the reduction of n, resulting in enhanced convective heat (Nu) and mass (Sh) exchange rates. For the apparent viscosity (μ_{CY}) at Figure 5(d), it remains constant for the same shear rate across the layer along the vertical axis.

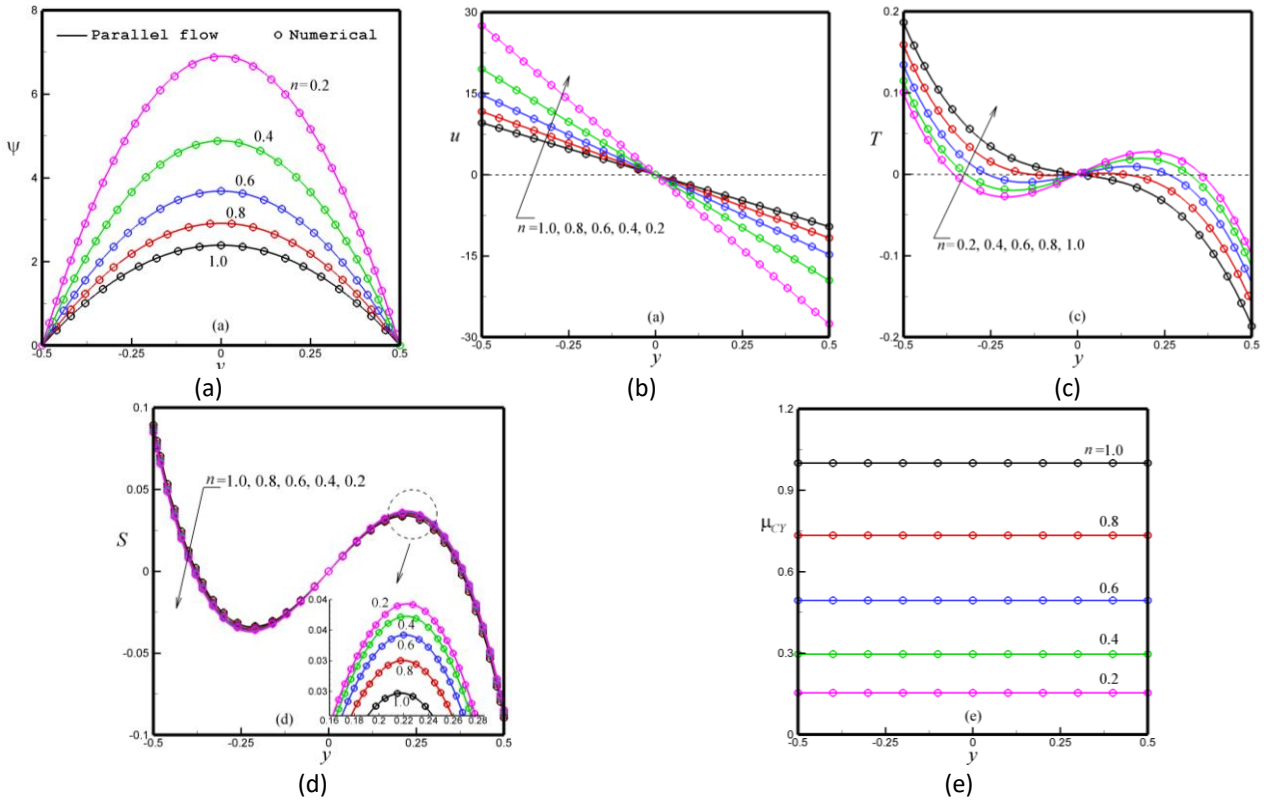

(a) (b) (c) (d) (e)

Fig. 5. Effect of n, on (a) ψ, (b) u, (c) T, (d) S, and (e) μ_{CY}, profiles at the mid-width of the porous layer ($x = 0$) $R_T = 50$, $Le = 5$, $\varphi = -0.1$, $\lambda_{CY} = 0.2$, $a = 2$, $s = 10^{-2}$, $\varepsilon = 1$

The impact of *Le* on R_{TC}^{sub} is depicted in Figure 6(a) for $\lambda_{CY} = 0.2$, $a = 2$, $s = 10^{-2}$, $\varphi = -0.1$, $\varepsilon = 1$, and different n. For $n = 1$, the same evolution of R_{TC}^{sub} and R_{TC}^{sup} vs. Le was reported by Rebhi *et al.*, [19]. As *Le* decreases from 10^3 to 2.16, R_{TC}^{sub} increases until reaching a peak ($R_{TC}^{sub} = 16$) at $Le = 3.2$, then it decreases toward $R_{TC}^{sub} = R_{TC}^{sup} = 15.32$ as$Le \to Le_C(2.16)$. Below this value ($Le \leq Le_C(2.16)$), the subcritical convection is not possible since the mass exchange through the porous layer is realized by pure diffusion. However, the onset of motion is supercritical (R_{TC}^{sup}) in the range ($Le_C(2.16) \leq Le \leq 10^{-2}$). The reduced n from ($1 \leq n \leq 0.2$) leads to a decrease in the threshold of subcritical Rayleigh convection. A significant change in the peaks of R_{TC}^{sub} are observed for different n. At $n = 1$ and 0.2, the peaks happen at $Le = 3.2$ and 1.6, respectively.

Figure 6(b) illustrates the changes in the critical Lewis number, Le_C (i.e., when$R_{TC}^{sub} = R_{TC}^{sup}$), as function of n. As observed, the reduced n from 1 to 0.56 yields a sharp decrease in Le_C. Below $n \leq 0.56$, the threshold of supercritical convection (R_{TC}^{sup}) disappears completely and the only existing critical Rayleigh number is the subcritical one (R_{TC}^{sub}).

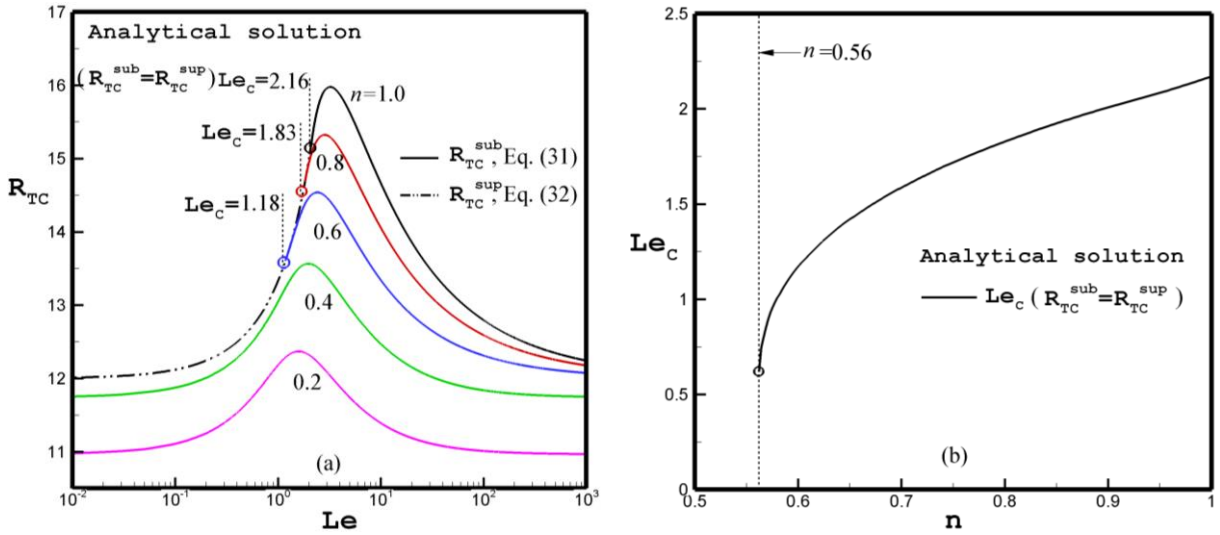

Fig. 6. Subcritical Rayleigh number, R_{TC}^{sub}, and supercritical Rayleigh number, R_{TC}^{sup}, as function of Le, and various values of n, for $\varphi = -0.1$, $\lambda_{CY} = 0.2$, $a = 2$ and $s = 10^{-2}$

Figure 7 shows the distribution of ψ_0 at the cavity center, Nu, Sh, and μ_{CY} versus Le and n for $R_T = 50$, $\varphi = -0.8$, $\lambda_{CY} = 0.2$, $a = 2$, $s = 10^{-2}$ and $\varepsilon = 1$. For $Le < 1$, the only possible solution is stable and the small amount of n induces oscillatory flows. In addition, the convection strength becomes large for $n = 0.4$ and $Le > 32$. For $0.95 \leq Le \leq 1.53$, the rest state prevails since $R_T = 50$ is below (R_{TC}^{sub}) for the convective motion. At $Le = 1.53$ and 0.95, the bifurcation from conductive to convective regime occurs ($\psi_0 = 1.74$, $Nu = 2.06$, $Sh = 2.93$ and $\mu_{CY} = 0.52$ for $Le = 1.53$ and $\psi_0 = 0.00$, $Nu = Sh = \mu_{CY} = 1.00forLe = 0.95$). It is seen from Figure 7(a) and Figure 7(b) that, as the Lewis number increases (decrease) above (below) $Le = 1.53$ (0.95), the strength of the convective motion and the thermal exchange rate augments continually until reaching a constant value as $Le \to \infty$ and $Le \to 0$, depending on n. For $Le < 1$, Sh increases until a peak, then it decreases toward $Sh = 1$, where this value is not affected by n, Figure 7(c). This is due to the considerable amount of mass diffusion coefficient and the diffusion domination in the field of species concentration. The heat is the lowest diffusive component when $Le < 1$, so the thermal exchange is mainly realized by convection, Figure 7(b) and Figure 7(c). Figure 8 highlights the changes in R_{TC}^{sub}, R_{TC}^{tur} and R_{TC}^{sup} with the buoyancy ratio (φ) for $Le = 5$, $\lambda_{CY} = 0.2$, $a = 2$ and $s = 10^{-2}$. The graph indicates that in the range ($-0.1 \leq \varphi \leq 0.1$), the subcritical Rayleigh number decreases with decreasing buoyancy ratio for various, n, thus the buoyancy ratio has a destabilizing effect.

At $\varphi = 0$, it is found that $R_{TC}^{sub} = R_{TC}^{sup} = 12$. Upon keeping the decrease in n and increase in the buoyancy ratio ($\varphi > 0$), the bi-stability phenomenon happens regardless of n. However, the extent of the bistability region depends on n, and it arises when the system has two steady-state solutions at the same conditions. In this case, a bi-stability region is formed between the two turning saddle-node points R_{TC}^{sub} and R_{TC}^{tur}, as illustrated in the zoom presented in Figure 8.

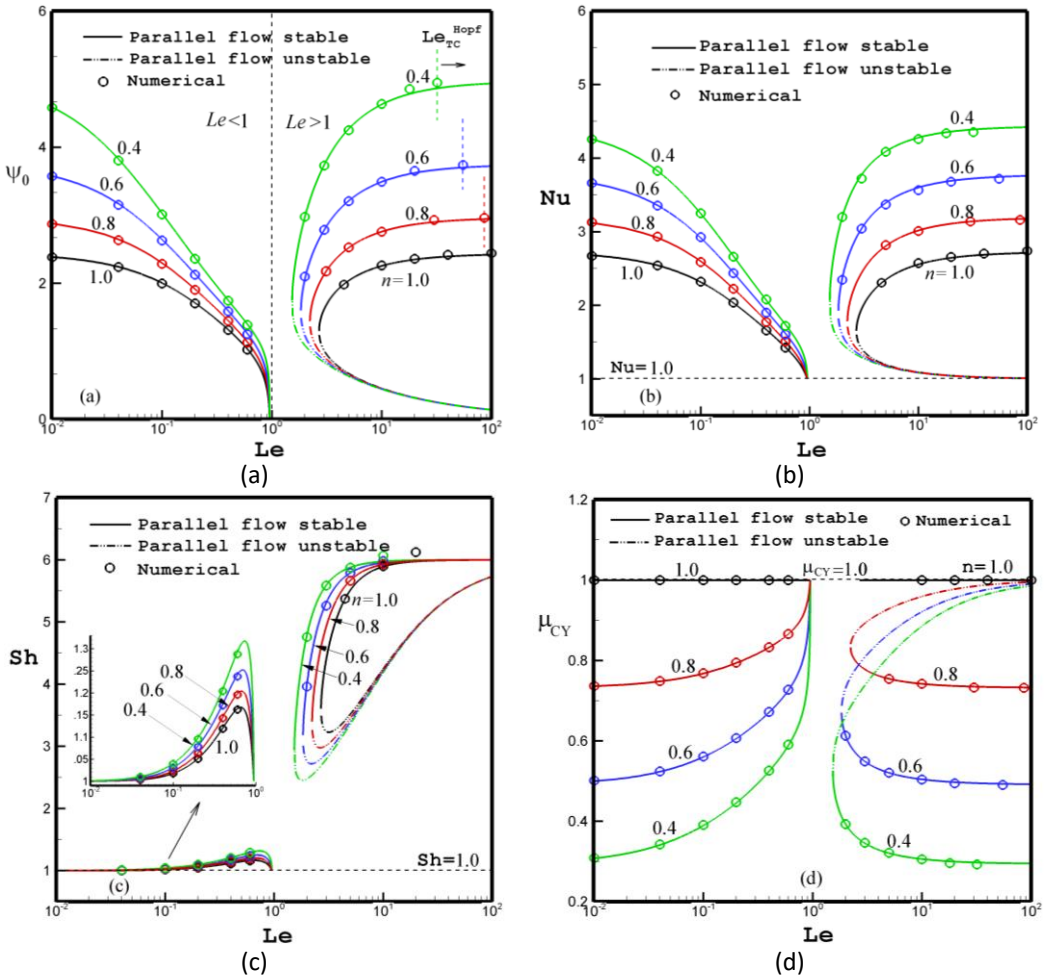

Fig. 7. The effect of Le and n, on (a) ψ_0, Nu, (c) Sh, and (d) μ_{CY}, for $R_T = 50$, $\varphi = -0.8$, $\lambda_{CY} = 0.2$, $a = 2$, $s = 10^{-2}$ and $\varepsilon = 1$

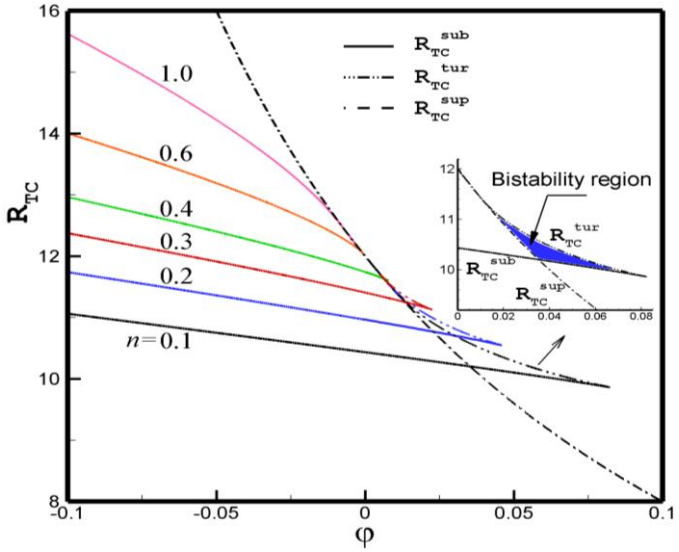

Fig. 8. Buoyancy ratio, φ, and n, effects on R_{TC}^{sup}, R_{TC}^{sub} and R_{TC}^{tur} for $Le = 5$, $\lambda_{CY} = 0.2$, $a = 2$ and $s = 10^{-2}$

When $n = 0.1$, in the range ($-0.1 \leq \varphi \leq 0.035$), R_{TC}^{sub} is the lowest, i.e., ($R_{TC}^{sub} < R_{TC}^{sup} < R_{TC}^{tur}$), as given in Figure 9. As observed, $R_{TC}^{sub} = R_{TC}^{sup} = 10.2$ at $\varphi = 0.035$. Even with the decrease of φ, there is a bi-stability in the range ($0.035 \leq \varphi \leq 0.082$). For this situation, the bifurcation curve consists of lower and upper supercritical branches that exist for $R_T \geq R_{TC}^{sub}$, as highlighted in Figure 9 for $\varphi = 0.04$. For this value, the bifurcation curve is particular and the onsets of motion are given by $R_{TC}^{sup} = 10$, $R_{TC}^{sub} = 10.17$ and $R_{TC}^{tur} = 10.47$. Two different stable branches are observed; the upper branch that starts at R_{TC}^{sub} is a subcritical bifurcation, while the lower branch corresponds to a supercritical bifurcation. However, it is observed that the lower stable branch exists only in the range ($R_{TC}^{sup} \leq R_T \leq R_{TC}^{tur}$), where R_{TC}^{tur} corresponds to a turning saddle-node point.

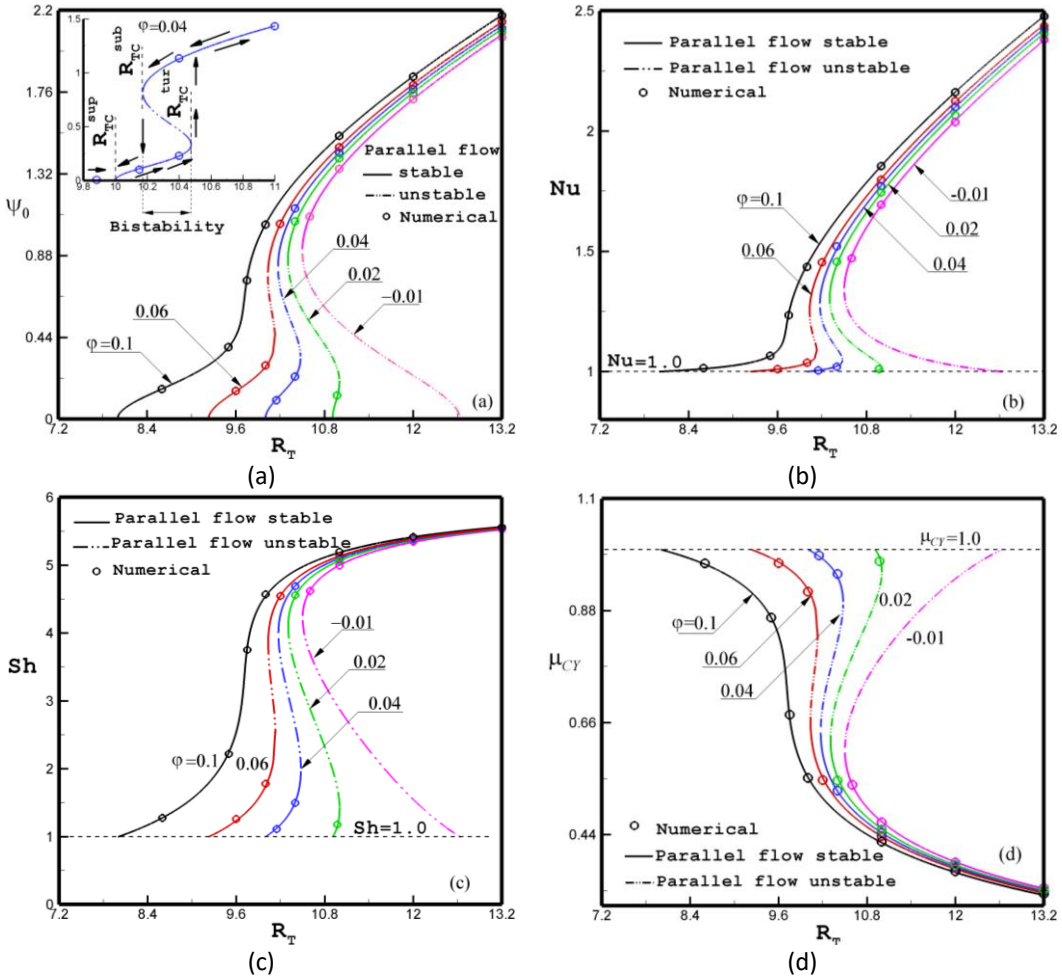

Fig. 9. Bifurcation diagram as a function of R_T and φ for $Le = 5$, $n = 0.1$, $\lambda_{CY} = 0.2$, $a = 2$, $s = 10^{-2}$and $\varepsilon = 1$, (a) ψ_0, (b) Nu, (c) Sh and (d) μ_{CY}

Figure 10(a) and Figure 10(b) presents the streamlines (ψ), thermal distribution (T), iso-concentration (S), and apparent viscosity (μ_{CY}) obtained for $R_T = 10.4$, $n = 0.1$ and $\varphi = 0.04$. The results obtained for $\varphi = 0.082$ indicate that the condition $R_{TC}^{sub} = R_{TC}^{tur} = 9.86$ is reached. For $0.082 \leq \varphi \leq 0.1$, there is only a supercritical Rayleigh number. The impact of the rheological index n ($0.1 \leq n \leq 1$) on the bi-stability region is illustrated in Figure 11 at $Le = 5$, $\varphi = 0.02$, $\lambda_{CY} = 0.2$, $a = 2$, $s = 10^{-2}$ and $\varepsilon = 1$. The results are qualitatively identical to those plotted in Figure 9 while studying the buoyancy ratio impact. There is a development of the bifurcation from the subcritical to the supercritical behavior, even with decreasing n. As already mentioned, the supercritical Rayleigh number is not affected by the n values and it remains at $R_{TC}^{sup} = 10.90$.

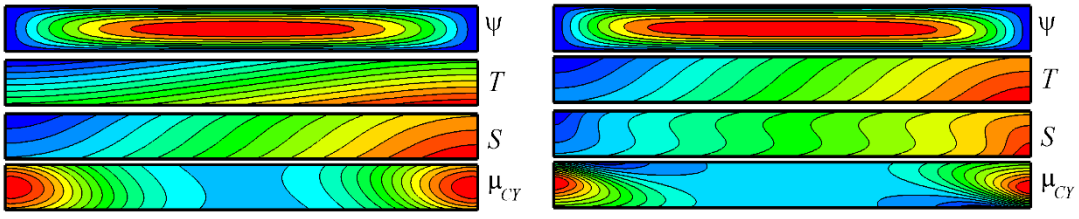

Fig. 10. Contours of stream, ψ, temperature, T, concentration, S, and apparent viscosity, μ_{CY}, for $R_T = 10.4$, $\varphi = 0.04$, $Le = 5$, $n = 0.1$, $\lambda_{CY} = 0.2$, $a = 2$, $s = 10^{-2}$and $\varepsilon = 1$: (a) $\psi_0 = 0.214$, $Nu = 1.020$, $Sh = 1.460$, $\mu_{CY} = 0.952$; (b) $\psi_0 = 1.141$, $Nu = 1.518$, $Sh = 4.687$, $\mu_{CY} = 0.521$

For intermediate values of n, the bifurcation profiles mean the presence of stable supercritical and subcritical parts connected by an unstable one, as highlighted by the curve for $\varphi = 0.04$ depicted in Figure 9, showing again the zone where the bi-stability convection happens. A bistability diagram ($R_{TC} - n$) is presented in Figure 11(e), where the bi-stability zone is highlighted by the hatched area.

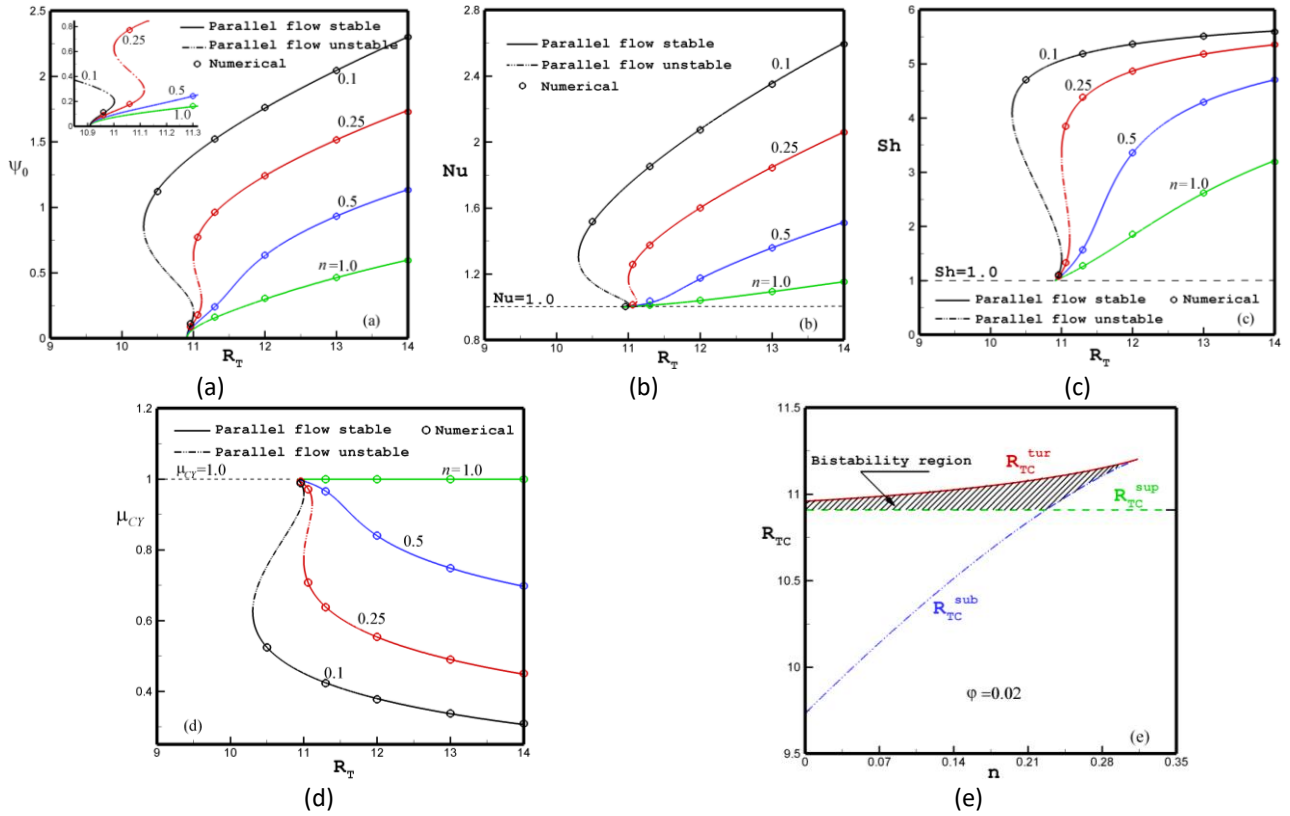

Fig. 11. Bifurcation diagram in terms of (a) ψ_0, (b) Nu, (c) Sh and (d) μ_{CY} versus n and R_T for $Le = 5$, $\varphi = 0.02$, $\lambda_{CY} = 0.2$, $a = 2$, $s = 10^{-2}$ and $\varepsilon = 1$. (e) Stability diagram showing the bistability region (hatched)

The effect of rheological parameters on the bi-stability zone is presented in Figure 12(a) to Figure 12(d) for $Le = 5$. Even with increasing/decreasing buoyancy ratio, the rheological parameters are increasingly affecting the bi-stability zone. The evolution of the bistability zone with λ_{CY} and s in Figure 12(a) and Figure 12(b) is comparable to that outlined in Figure 8. In general, upon increasing/decreasing progressively from zero the material time constant, λ_{CY}, (parameter, s) the bi-stability zone is reduced, and it disappears completely at $\lambda_{CY} = 0$ and $s = 1$. In Figure 12(c), the curve obtained for $a = 1$ to 2 are the same as those discussed above for Figure 12(a) and Figure 12(b). R_{TC}^{tur} becomes less than R_{TC}^{sup} since it degenerates into a second turning point R_{TC}^{tur2}. For the range

$(-0.019 \leq \varphi \leq -0.032)$ and even with the rise of the buoyancy ratio, the bifurcation profile has an upper supercritical part extending between $(R_{TC}^{sup} \leq R_T \leq R_{TC}^{tur1})$ and a lower part existing at the condition $R \leq R_{TC}^{tur2}$. This point was not observed with the change of n, λ_{CY}, and s. The results obtained at $\varphi = -0.032$, for which $R_{TC}^{tur1} = R_{TC}^{tur2} = 13.55$, and at $\varphi = -0.019$ ($\varphi = -0.009$) are $R_{TC}^{tur1} = R_{TC}^{sup} = 13.26$ ($R_{TC}^{tur2} = R_{TC}^{sup} = 12.56$).

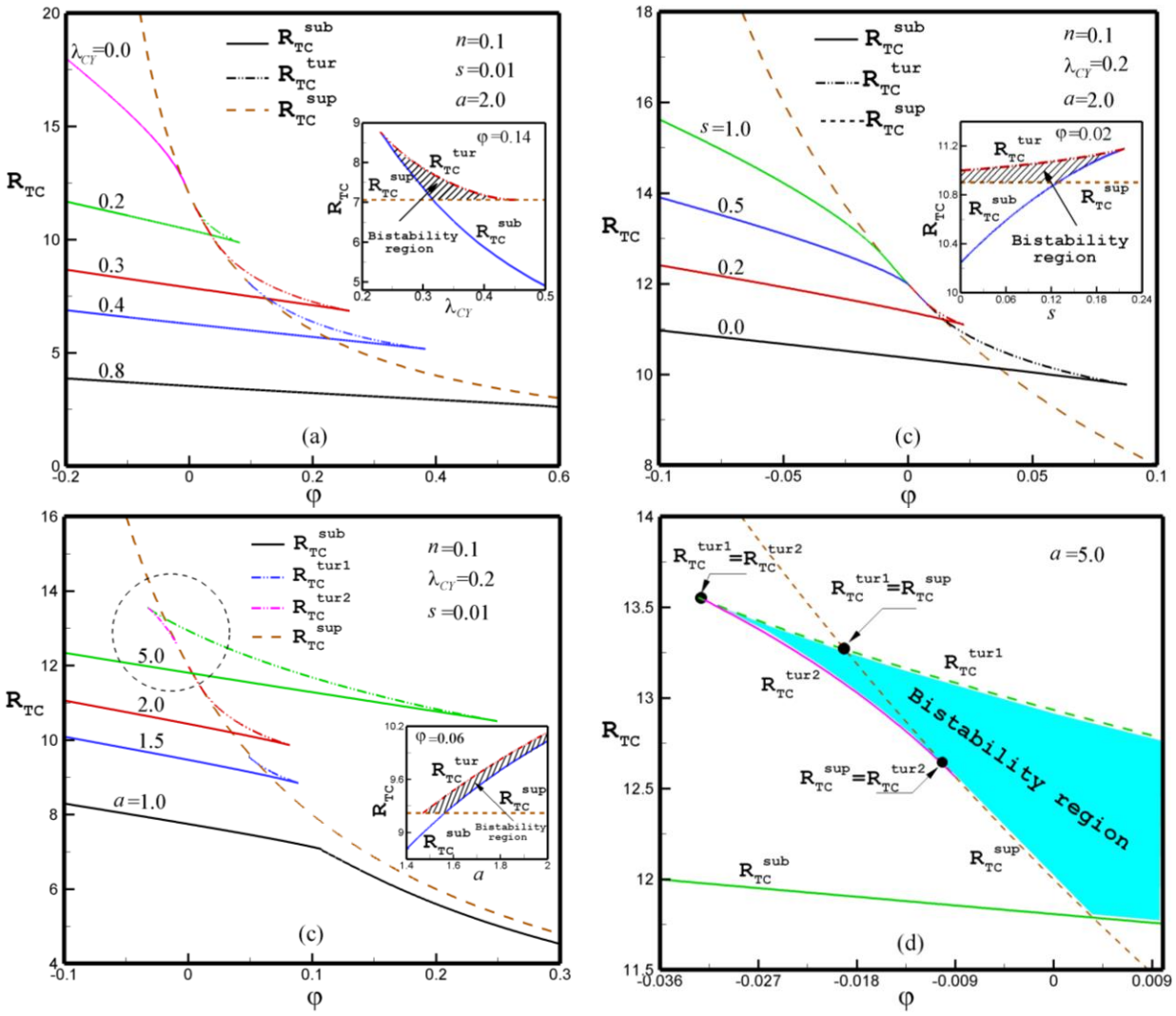

Fig. 12. Effect of varying the Carreau-Yasuda parameters (λ_{CY}, s and a) and the buoyancy ratio, φ, on the bistability region for$Le = 5$

The impact of φ is illustrated in Figure 13(a) to Figure 13(d). It has been analytical predicted that the bifurcation is subcritical at $\varphi = -0.035$. Upon decreasing the buoyancy ratio between $(-0.035 \leq \varphi \leq 0)$, the bifurcation behavior undergoes a remarkable change. It is noted from Figure 13 that in the range $(-0.03 \leq \varphi \leq -0.01)$, four solutions may be obtained (two stable and two unstable), which confirms the presence of bi-stability. The graph obtained at $\varphi = -0.02$ in Figure 13(a) means the presence of two stable parts. The upper part beginning from R_{TC}^{sub} is the standard part remarked in the subcritical bifurcation existing when $R_T \geq R_{TC}^{sub} = 11.91$. While the lower stable part that starts at $R_{TC}^{tur2} = 13.11$ corresponds to a turning bifurcation. In addition, the lower part is present within the range $(R_{TC}^{tur2} \leq R_T \leq R_{TC}^{tur1})$, where $R_{TC}^{tur1} = 13.28$. The stable parts (upper and lower) are connected by an upper unstable part, plotted as a dotted line. There is also a lower unstable branch extending between $(R_{TC}^{sup}(13.33) \leq R_T \leq R_{TC}^{tur2}(13.11))$, which is due to the

buoyancy effect. This type of bifurcation is being similar to that depicted in Figure 11 while studying the effect of n.

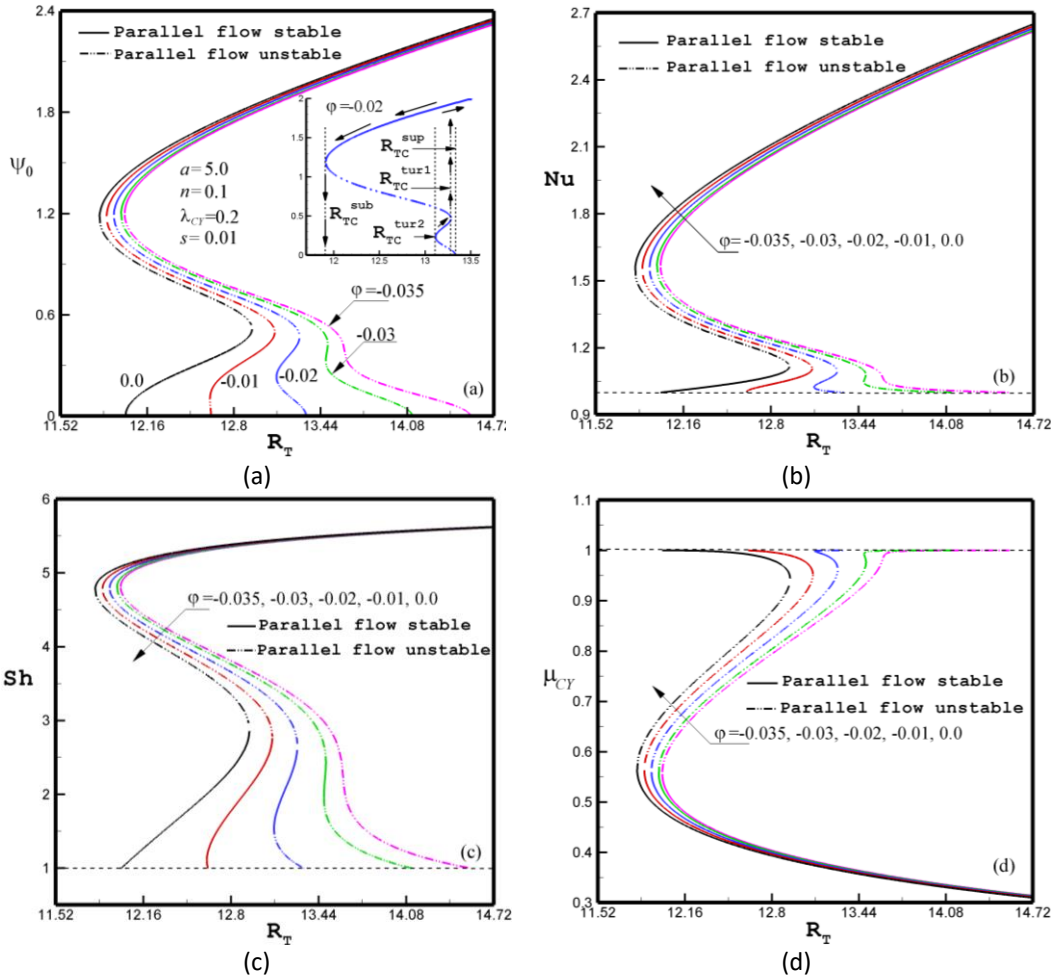

(a) (b) (c) (d)

Fig. 13. Bifurcation diagram as a function of R_T and φ for$Le = 5$, $a = 5$, $n = 0.1$, $\lambda_{CY} = 0.2$ and$s = 10^{-2}$, (a) ψ_0, (b) Nu, (c) Sh and (d) μ_{CY}

The combination of the parallel flow and linear stability approaches was performed to reveal the impact of the buoyancy ratio (φ) on the thresholds of bifurcation (R_{TC}^{sub}, R_{TC}^{tur1}, R_{TC}^{tur2}, R_{TC}^{sup}, R_{TC}^{over}, R_{TC}^{osc} and R_{TC}^{Hopf}) for $Le = 5$ and $\varepsilon = 1$, Figure 14. The values of R_{TC}^{sup}, R_{TC}^{over}, R_{TC}^{osc}, and R_{TC}^{Hopf} are determined by the linear stability theory of the rest state and the convective state described in section (5), while the values of R_{TC}^{sub}, R_{TC}^{tur1}, and R_{TC}^{tur2} are determined by the nonlinear parallel flow approximation, (Eq. (32)). The stability diagrams plotted in Figure 14(a) and Figure 14(b) are characterized by seven different zones. The first bifurcation zone (I) is located between the two points, where a subcritical bifurcation occurs and being connected to a supercritical bifurcation. For this region, the convective flow is at a rest state. In zone (II), when $R_{TC}^{sub} \leq R_T \leq R_{TC}^{over}$, the linear stability theory predicts a stable rest state. Zone (III) is characterized by the existence of a bi-stability region leading to three solutions (two stable and one unstable) or four solutions (two stable and two unstable), as those discussed above for Figure 13. Thus, for $R_{TC}^{over} \leq R_T \leq R_{TC}^{osc}$, zone (IV), the linear stability theory predicts the possible existence of oscillating flow pattern, delineated by $R_{TC}^{over}$and oscillatory R_{TC}^{osc}. For this zone, the convection is amplified in an oscillatory manner. It is also observed that, for $\varphi = -0.04$, the condition for a codimension-2 points are reached ($R_{TC}^{over} = R_{TC}^{osc} = R_{TC}^{sup}$). Below this limit, the overstability regime does not exist. In region (V), delineated by $R_{TC}^{osc} \leq R_T \leq$

R_{TC}^{sup}, the system remains oscillatory. In region (VI), delineated by $R_{TC}^{sup} \leq R_T \leq R_{TC}^{Hopf}$, the system is unstable. For $R_T \geq R_{TC}^{Hopf}$, the region (VII) presets the oscillatory finite amplitude convection that begins just above the threshold for Hopf bifurcation.

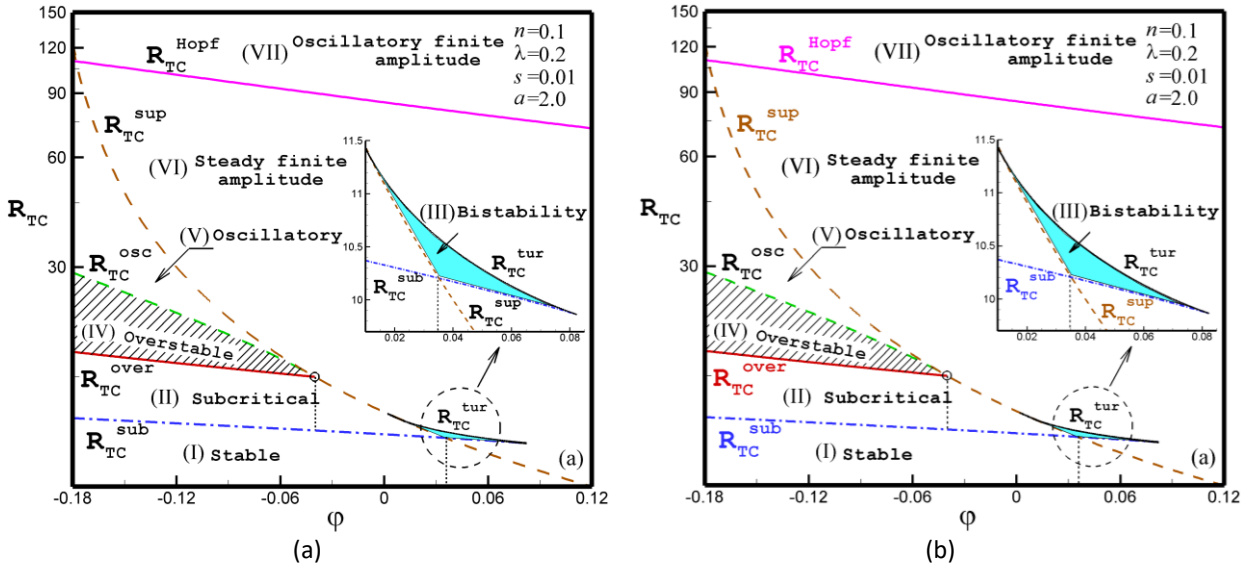

Fig. 14. Stability diagrams in the $R_{TC} - \varphi$ plane for $Le = 5$, $n = 0.1$, $\lambda_{CY} = 0.2$ and $\varepsilon = 1$: (a) $a = 2$ and (b) $a = 5$

Further insight into the effects of φ on the onset of motion is provided by Figure 15. As expected, the buoyancy ratio had a strong influence on the critical Rayleigh number. Zone (I)-(VII) are equivalent to those given in Figure 14.

The solutions corresponding to the upper and lower stable branches, Figure 15(a) to Figure 15(d), may be reached only according to the hysteresis path plotted on the profile.

The variation of the thresholds of bifurcation (R_{TC}^{sub}, R_{TC}^{over}, R_{TC}^{osc}, R_{TC}^{sup} and R_{TC}^{Hopf}) with the normalized porosity, ε, is depicted in Figure 16 for $Le = 5$, $\varphi = -0.1$, $n = 0.1$, $\lambda_{CY} = 0.2$, $s = 10^{-2}$ and $a = 5$. For this case, $R_{TC}^{sup} = 24$ and $R_{TC}^{sub} = 12.40$, which are influenced by the normalized porosity. Upon decreasing the normalized porosity below ($\varepsilon \leq 1$), the graph indicates the existence of an over-stability region (R_{TC}^{over}). This region ex ıds up to $\varepsilon = 0.4$, at which point the condition $R_{TC}^{sup} = R_{TC}^{over} = R_{TC}^{osc}$ is reached. For $\varepsilon < 0.4$, the over-stability region (zone III) disappears completely.

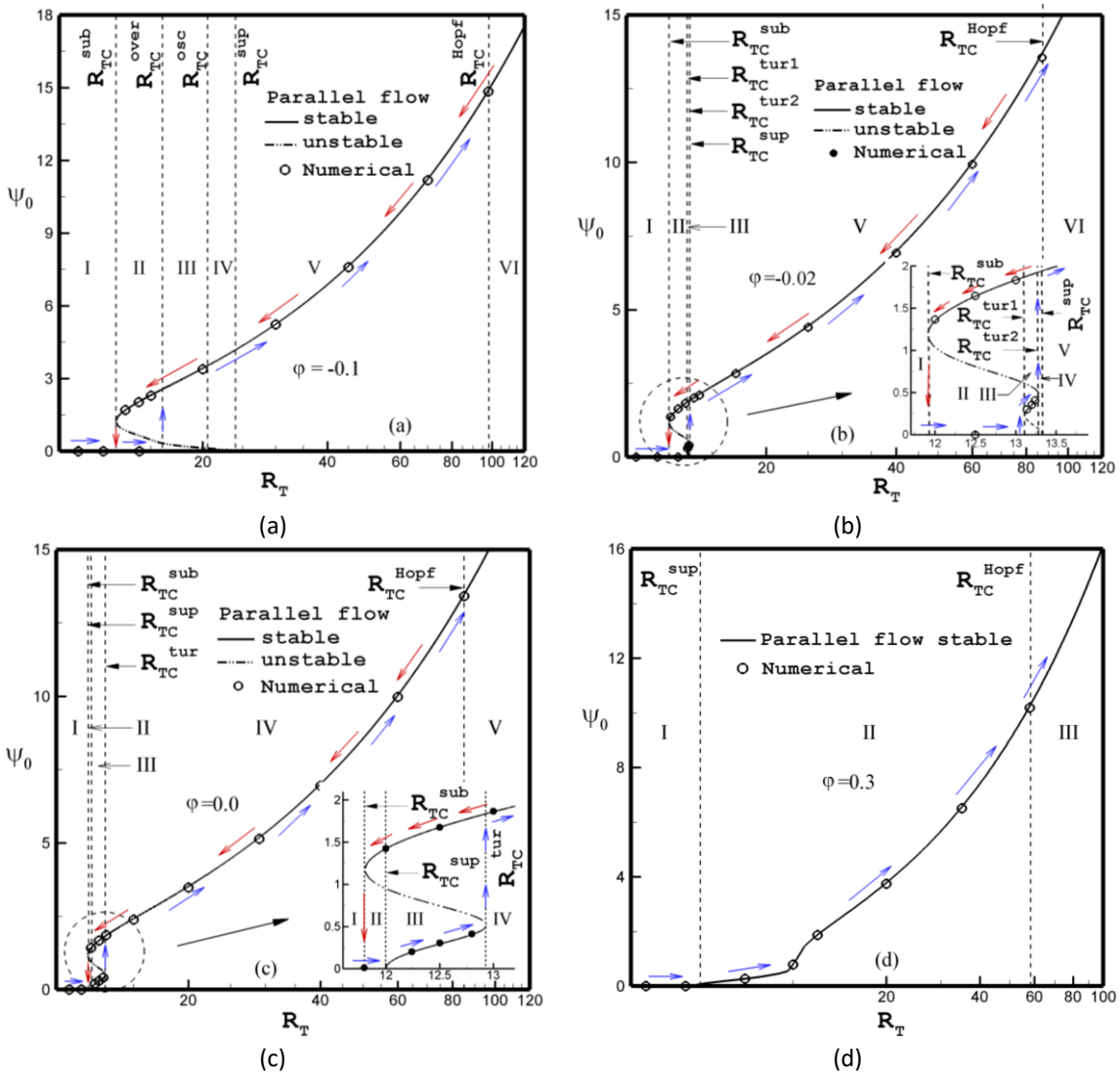

Fig. 15. Bifurcation diagram in terms of ψ_0 versus φ and R_T for $Le = 5$, $n = 0.1$, $\lambda_{CY} = 0.2$, $a = 2$ and $s = 10^{-2}$

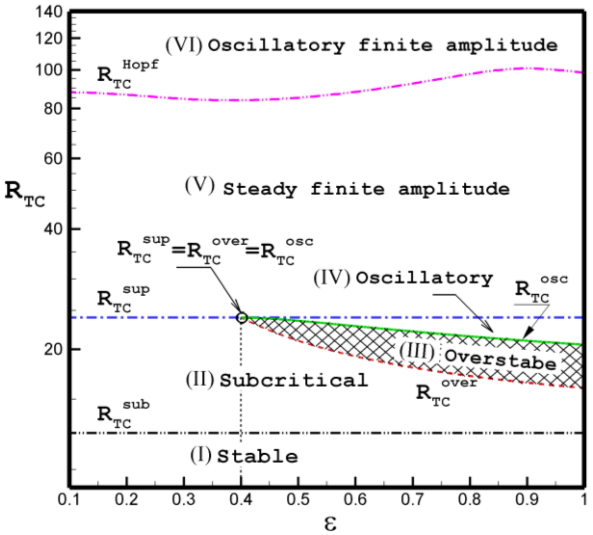

Fig. 16. Stability diagram in the $(R_{TC} - \varepsilon)$ plane for $Le = 5$, $\varphi = -0.1$, $n = 0.1$, $\lambda_{CY} = 0.2$, $s = 10^{-2}$ and $a = 5$

7. Conclusion

The natural convection with double diffusive in a porous layer saturated with a non-Newtonian fluid and subjected to a constant heat from the bottom was examined. The main conclusions of the current study are the following

i. For an infinite layer, a good comparison was obtained between the findings of the parallel flow theory and the numerical technique. The strength of convection (ψ_0), thermal and mass exchange rates (Nu and Sh) are intensified when ($0.1 \leq n \leq 1$) or ($0 \leq \lambda_{CY} \leq 1$). A similar trend is found for viscosity apparent (μ_{CY}) with the rise or decrease of n and λ_{CY}. For a significant Rayleigh number, the thermal and mass exchange rates become constant $Nu(Sh) \to 6.0$, and this independently of the value of both n and λ_{CY}.
ii. With the rise of decrease of φ, the bi-stability region was more and more affected by the rheological parameters of Carreau-Yassuda. The bistability region was found to shrinks and it disappears when increasing the values of n and s, or when decreasing the time constant, λ_{CY} and the parameter a.
iii. As expected, an enhancement in the shear-thinning behavior is observed upon decreasing/increasing time constant (λ_{CY}), which leads to the early appearance of subcritical convection. Thus, an increase of n, s and decrease of λ_{CY}, the threshold of subcritical convection (R_{TC}^{sub}) increases monotonously towards a constant value, independently of n, s, and λ_{CY}. However, when the increasing of parameter, a, the threshold of subcritical convection behavior had slightly different from those observed for n, s and λ_{CY}.
iv. Regarding the diffusive state stability and for an infinite horizontal layer, the onset of motion from the rest state (R_{TC}^{sup}, R_{TC}^{over}, R_{TC}^{osc}) depends on Le, φ, ε and rheological parameters (n, λ_{CY}, a and s).
v. For given values of Le, φ and ε, the onset of motion from the rest state (R_{TC}^{sup}, R_{TC}^{over}, R_{TC}^{osc}) is not affected by n and s, but the time constant, λ_{CY}, and the parameter, a, had a significant effect. When the fluid became more and more shear-thinning, both the onset of subcritical convection and Hopf bifurcation is reduced, which played the role of a destabilizing flow parameter.

References

[1] Escudier, M. P., R. J. Poole, F. Presti, C. Dales, C. Nouar, C. Desaubry, L. Graham, and L. Pullum. "Observations of asymmetrical flow behaviour in transitional pipe flow of yield-stress and other shear-thinning liquids." *Journal of Non-Newtonian Fluid Mechanics* 127, no. 2-3 (2005): 143-155. https://doi.org/10.1016/j.jnnfm.2005.02.006
[2] Piau, J. M., N. El Kissi, and B. Tremblay. "Low Reynolds number flow visualization of linear and branched silicones upstream of orifice dies." *Journal of Non-Newtonian Fluid Mechanics* 30, no. 2-3 (1988): 197-232. https://doi.org/10.1016/0377-0257(88)85025-0
[3] Hadidi, N., and R. Bennacer. "Three-dimensional double diffusive natural convection across a cubical enclosure partially filled by vertical porous layer." *International Journal of Thermal Sciences* 101 (2016): 143-157. https://doi.org/10.1016/j.ijthermalsci.2015.10.029
[4] Davis, G. de Vahl. "Natural convection of air in a square cavity: a bench mark numerical solution." *International Journal for Numerical Methods in Fluids* 3, no. 3 (1983): 249-264. https://doi.org/10.1002/fld.1650030305
[5] Beghein, C., F. Haghighat, and F. Allard. "Numerical study of double-diffusive natural convection in a square cavity." *International Journal of Heat and Mass Transfer* 35, no. 4 (1992): 833-846. https://doi.org/10.1016/0017-9310(92)90251-M
[6] Ostrach, Simon. "Natural convection with combined driving forces." *Physicochemical Hydrodynamics* 1, no. 4 (1980): 233-247.

[7] Ostrach, Simon. "Natural convection in enclosures." *Journal of Heat and Mass Transfer* 110, no. 4b (1988): 1175-1190. https://doi.org/10.1115/1.3250619
[8] Bejan, Adrian. *Convection heat transfer*. Third ed. John Wiley & Sons, 2004.
[9] Goyeau, B., J-P. Songbe, and D. Gobin. "Numerical study of double-diffusive natural convection in a porous cavity using the Darcy-Brinkman formulation." *International Journal of Heat and Mass Transfer* 39, no. 7 (1996): 1363-1378. https://doi.org/10.1016/0017-9310(95)00225-1
[10] Gobin, D., and R. Bennacer. "Cooperating thermosolutal convection in enclosures-II. Heat transfer and flow structure." *International Journal of Heat and Mass Transfer* 39, no. 13 (1996): 2683-2697. https://doi.org/10.1016/0017-9310(95)00351-7
[11] Chen, Falin, and C. F. Chen. "Convection in superposed fluid and porous layers." *Journal of Fluid Mechanics* 234 (1992): 97-119. https://doi.org/10.1017/S0022112092000715
[12] Zhao, Pinghua, and C. F. Chen. "Stability analysis of double-diffusive convection in superposed fluid and porous layers using a one-equation model." *International Journal of Heat and Mass Transfer* 44, no. 24 (2001): 4625-4633. https://doi.org/10.1016/S0017-9310(01)00102-8
[13] Valencia-Lopez, J. J., and J. A. Ochoa-Tapia. "A study of buoyancy-driven flow in a confined fluid overlying a porous layer." *International Journal of Heat and Mass Transfer* 44, no. 24 (2001): 4725-4736. https://doi.org/10.1016/S0017-9310(01)00105-3
[14] Serrano-Arellano, J., J. Xamán, G. Álvarez, and M. Gijón-Rivera. "Heat and mass transfer by natural convection in a square cavity filled with a mixture of Air-CO_2." *International Journal of Heat and Mass Transfer* 64 (2013): 725-734. https://doi.org/10.1016/j.ijheatmasstransfer.2013.05.038
[15] Kalla, L., M. Mamou, P. Vasseur, and L. Robillard. "Multiple solutions for double diffusive convection in a shallow porous cavity with vertical fluxes of heat and mass." *International Journal of Heat and Mass Transfer* 44, no. 23 (2001): 4493-4504. https://doi.org/10.1016/S0017-9310(01)00076-X
[16] Bahloul, A., N. Boutana, and P. Vasseur. "Double-diffusive and Soret-induced convection in a shallow horizontal porous layer." *Journal of Fluid Mechanics* 491 (2003): 325-352. https://doi.org/10.1017/S0022112003005524
[17] Bahloul, A., P. Vasseur, and L. Robillard. "Convection of a binary fluid saturating a shallow porous cavity subjected to cross heat fluxes." *Journal of Fluid Mechanics* 574 (2007): 317-342. https://doi.org/10.1017/S0022112006004113
[18] Mamou, Mahmoud. "Stability analysis of the perturbed rest state and of the finite amplitude steady double-diffusive convection in a shallow porous enclosure." *International Journal of Heat and Mass Transfer* 46, no. 12 (2003): 2263-2277. https://doi.org/10.1016/S0017-9310(02)00523-9
[19] Rebhi, Redha, Mahmoud Mamou, Patrick Vasseur, and Mounir Alliche. "Form drag effect on the onset of non-linear convection and Hopf bifurcation in binary fluid saturating a tall porous cavity." *International Journal of Heat and Mass Transfer* 100 (2016): 178-190. https://doi.org/10.1016/j.ijheatmasstransfer.2016.04.060
[20] Rebhi, Redha, Mahmoud Mamou, and Patrick Vasseur. "Bistability and hysteresis induced by form drag in nonlinear subcritical and supercritical double-diffusive Lapwood convection in shallow porous enclosures." *Journal of Fluid Mechanics* 812 (2017): 463-500. https://doi.org/10.1017/jfm.2016.787
[21] Attia, Abbes, Mahmoud Mamou, Smail Benissaad, and Nabil Ouazaa. "Linear and nonlinear stability of Soret-Dufour Lapwood convection near double codimension-2 points." *Heat Transfer-Asian Research* 48, no. 3 (2019): 763-792. https://doi.org/10.1002/htj.21405
[22] Bian, W., Patrick Vasseur, and E. Bilgen. "Natural convection of non-Newtonian fluids in an inclined porous layer." *Chemical Engineering Communications* 129, no. 1 (1994): 79-97. https://doi.org/10.1080/00986449408936252
[23] Pericleous, K. A. "Heat transfer in differentially heated non-newtonian cavities." *International Journal of Numerical Methods for Heat & Fluid Flow* 4, no. 3 (1994): 229-248. https://doi.org/10.1108/EUM0000000004040
[24] Chen, Han Taw, and Cha'O Kuang Chen. "Free convection flow of non-newtonian fluids along a vertical plate embedded in a porous medium." *Journal of Heat Transfer* 110, no. 1 (1988): 257-260. https://doi.org/10.1115/1.3250462
[25] Mehta, K. N., and K. Narasimha Rao. "Buoyancy induced flow of non-Newtonian fluids over a non-isothermal horizontal plate embedded in a porous medium." *International Journal of Engineering Science* 32, no. 3 (1994): 521-525. https://doi.org/10.1016/0020-7225(94)90138-4
[26] Mehta, K. N., and K. Narasimha Rao. "Buoyancy-induced flow of non-Newtonian fluids in a porous medium past a vertical flat plate with nonuniform surface heat flux." *International Journal of Engineering Science* 32, no. 2 (1994): 297-302. https://doi.org/10.1016/0020-7225(94)90009-4
[27] Getachew, D., D. Poulikakos, and W. J. Minkowycz. "Double diffusion in a porous cavity saturated with non-Newtonian fluid." *Journal of Thermophysics and Heat Transfer* 12, no. 3 (1998): 437-446. https://doi.org/10.2514/2.6357

[28] Lamsaadi, M., M. Naimi, and M. Hasnaoui. "Natural convection of non-Newtonian power law fluids in a shallow horizontal rectangular cavity uniformly heated from below." *Heat and Mass Transfer* 41, no. 3 (2005): 239-249. https://doi.org/10.1007/s00231-004-0530-8
[29] Khelifa, Nabil Ben, Zineddine Alloui, Hassen Beji, and Patrick Vasseur. "Natural convection in a vertical porous cavity filled with a non-newtonian binary fluid." *AIChE Journal* 58, no. 6 (2012): 1704-1716. https://doi.org/10.1002/aic.13815
[30] Lamsaadi, M., M. Naimi, M. Hasnaoui, and M. Mamou. "Natural convection in a vertical rectangular cavity filled with a non-Newtonian power law fluid and subjected to a horizontal temperature gradient." *Numerical Heat Transfer, Part A: Applications* 49, no. 10 (2006): 969-990. https://doi.org/10.1080/10407780500324988
[31] Benouared, Ouahiba, Mahmoud Mamou, and Noureddine Ait Messaoudene. "Numerical nonlinear analysis of subcritical Rayleigh-Bénard convection in a horizontal confined enclosure filled with non-Newtonian fluids." *Physics of Fluids* 26, no. 7 (2014): 073101. https://doi.org/10.1063/1.4890829
[32] Khechiba, Khaled, Mahmoud Mamou, Madjid Hachemi, Nassim Delenda, and Redha Rebhi. "Effect of Carreau-Yasuda rheological parameters on subcritical Lapwood convection in horizontal porous cavity saturated by shear-thinning fluid." *Physics of Fluids* 29, no. 6 (2017): 063101. https://doi.org/10.1063/1.4986794
[33] Rebhi, Redha, Mahmoud Mamou, and Patrick Vasseur. "Bistability and hysteresis induced by form drag in nonlinear subcritical and supercritical double-diffusive Lapwood convection in shallow porous enclosures." *Journal of Fluid Mechanics* 812 (2017): 463-500. https://doi.org/10.1017/jfm.2016.787
[34] Alloui, Z., and P. Vasseur. "Natural convection of Carreau-Yasuda non-Newtonian fluids in a vertical cavity heated from the sides." *International Journal of Heat and Mass Transfer* 84 (2015): 912-924. https://doi.org/10.1016/j.ijheatmasstransfer.2015.01.092
[35] Krishna, M. Veera, and G. Subba Reddy. "MHD forced convective flow of non-Newtonian fluid through stumpy permeable porous medium." *Materials Today: Proceedings* 5, no. 1 (2018): 175-183. https://doi.org/10.1016/j.matpr.2017.11.069
[36] Rebhi, Redha, Mahmoud Mamou, and Noureddine Hadidi. "Bistability bifurcation phenomenon induced by non-Newtonian fluids rheology and thermosolutal convection in Rayleigh-Bénard convection." *Physics of Fluids* 33, no. 7 (2021): 073104. https://doi.org/10.1063/5.0051058
[37] Lounis, Selma, Redha Rebhi, Noureddine Hadidi, Giulio Lorenzini, Younes Menni, Houari Ameur, and Nor Azwadi Che Sidik. "Thermo-Solutal Convection of Carreau-Yasuda Non-Newtonian Fluids in Inclined Square Cavities Under Dufour and Soret Impacts." *CFD Letters* 14, no. 3 (2022): 96-118. https://doi.org/10.37934/cfdl.14.3.96118
[38] Yasuda, K. Y., R. C. Armstrong, and R. E. Cohen. "Shear flow properties of concentrated solutions of linear and star branched polystyrenes." *Rheologica Acta* 20, no. 2 (1981): 163-178. https://doi.org/10.1007/BF01513059
[39] Vasseur, Patrick, M. G. Satish, and Luc Robillard. "Natural convection in a thin, inclined, porous layer exposed to a constant heat flux." *International Journal of Heat and Mass Transfer* 30, no. 3 (1987): 537-549. https://doi.org/10.1016/0017-9310(87)90268-7
[40] Mamou, M., and P. Vasseur. "Thermosolutal bifurcation phenomena in porous enclosures subject to vertical temperature and concentration gradients." *Journal of Fluid Mechanics* 395 (1999): 61-87. https://doi.org/10.1017/S0022112099005753